RSC Advances

PAPER

View Article Online
View Journal | View Issue

Cite this: *RSC Adv.*, 2016, **6**, 98356

Effect of carbon nanosheets with different graphitization degrees as a support of noble metals on selective hydrogenation of cinnamaldehyde†

Qing Han, Yunfei Liu, Dong Wang, Fulong Yuan, Xiaoyu Niu* and Yujun Zhu*

Received 14th July 2016
Accepted 8th October 2016

DOI: 10.1039/c6ra17979g

www.rsc.org/advances

In this work, Pt and Pd catalysts supported on carbon nanosheets (CNS) with different graphitization degrees were prepared *via* a simple borohydride reduction method. The effect of graphitization degree on the catalytic activity of Pt/CNS and Pd/CNS was investigated to obtain the optimal activity. The prepared catalysts were well characterized by X-ray diffraction (XRD), Raman, transmission electron microscopy (TEM) and X-ray photoemission spectroscopy (XPS). The activity and selectivity of Pt/CNS and Pd/CNS catalysts increases with the rise of the graphitization degree of CNS. A high graphitization degree of the CNS support can enhance the transfer of electrons from the CNS support to Pt and Pd nanoparticles, leading to the increase in the surface Pt^0 and Pd^0 content. The more surface Pt^0 and Pd^0 content the catalyst has, the higher selectivity to COL and CALD it exhibits, respectively. The good graphitization degree of the CNS support is an advantage of the strong π–π interactions between CAL and the surface sp^2-bonded of CNS support. Thus, the different catalytic activity and selectivity over the Pt/CNS and Pd/CNS catalysts are attributed to the surface Pt^0 and Pd^0 content and the adsorption *capacity* for CAL on the catalyst surface that are closely related to the graphitization degree of CNS.

Introduction

With the rapid development of catalyst science and technology, controlling reaction selectivity has becoming more and more significant.[1–3] As a typical example, selective hydrogenation of α,β-unsaturated aldehydes is a common interest point both in industrial and academic circles.[4–6] For example, cinnamaldehyde (CAL) hydrogenation can produce cinnamal alcohol (COL), hydrocinnamaldehyde (HALD), hydrocinnamal alcohol (HALC), and so on (Scheme 1).[7–11] Among them, COL is generally considered to be the most challenging one to achieve. Also, it is an important type of organic ingredient for chemical synthesis, such as perfumes, cosmetics, medicines, and fungicides.[12,13] The obtained COL still remains an arduous task because the C=C bond reduction is more favorable than that of the C=O functional group, thermodynamically. Therefore, high active catalysts for selective production are urgently desired.

Recently, plenty of homogeneous catalysts have been reported for selectively catalytic hydrogenation of CAL.[14–16] However, the difficulty to retrieve the dissolved metal ions from the chemical reaction vessel greatly hinders their widespread applications. To this end, heterogeneous catalysts have attracted lots of interest because they are environmental friendly and easy to be retrieved. Up to date, both noble metal (*e.g.*, Pt, Pd, Ir, and Ru) and non-noble metal (*e.g.*, Fe, Co, Ni and Cu) nanoparticles (NPs) have been proved as highly efficient catalysts for selectively producing COL and HALD.[17–26] Generally, Pt and Pd nanoparticles are considered as active metals for the hydrogenation of C=O and C=C bonds of CAL, respectively.[20,23] Nevertheless, these NPs still have some drawbacks such as spontaneous aggregation due to the high surface energy, limited adsorption ability resulted from low surface area and small pore volume, and readily contaminated catalytic active sites.[27–30] Therefore, anchoring nanoparticles on the supports

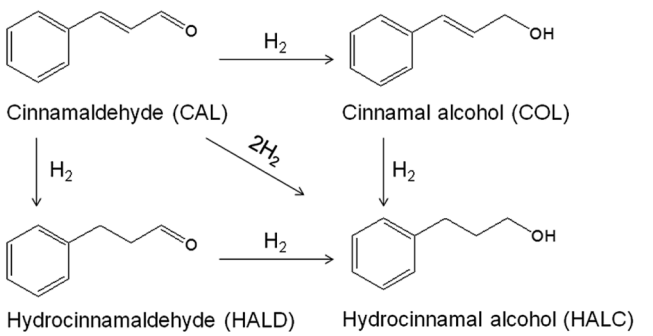

Scheme 1 Reaction pathways for cinnamaldehyde hydrogenation.

Key Laboratory of Functional Inorganic Material Chemistry (Heilongjiang University), Ministry of Education, School of Chemistry and Materials, Heilongjiang University, Harbin, 150080 P. R. China. E-mail: yujunzhu@hlju.edu.cn; niuxiaoyu2000@126.com; Fax: +86-451-86609650; Tel: +86-451-86609650

† Electronic supplementary information (ESI) available. See DOI: 10.1039/c6ra17979g

has been regarded to be a reasonable and reliable way to overcome the above mentioned difficulties.[31–35]

Various reducible metal oxides such as CeO_2,[36,37] MnO_2,[38] TiO_2 (ref. 39 and 40) and ZnO[41] have been used as the catalyst supports and found to be able to improve the selectivity to COL and HALD productions. Besides metal oxides, carbon material also has been demonstrated as a promising support for metal NPs towards hydrogenation of unsaturated aldehyde.[42–47] For example, Shi *et al.* found that reduced graphene oxide supported Pt catalysts exhibited excellent catalytic performances in terms of selectivity for the hydrogenation of unsaturated aldehydes.[42] In our previous report, the activity and selectivity may be related with the strong π–π interactions between cinnamaldehyde and graphene.[43] In addition, we also found the property of supports, addition of MoN and WN can influence the dispersion, content and valence state of the surface Pt and Pd species, resulting to the change of the activity and selectivity in hydrogenation of CAL.[16,25] So far, there are very few reports about the effect of carbon support nature on the catalytic performance for COL and HALD productions.

In this work, a series of carbon nanosheets (CNS) with different graphitization degree supported Pt and Pd catalysts were prepared through *in situ* self-generating template and post-loading two processes. The graphitization degree of CNS supports can be well controlled by the amount of growth catalysts (Fe species). The effect of CNS supports with different graphitization degree on catalytic performances of the Pt/CNS and Pd/CNS catalysts have been carefully studied for the selective hydrogenation of CAL.

Experimental

Material preparation

Synthesis of CNS support with different graphitization degree. As reported previously, the CNS supports were fabricated by an *in situ* self-generating template route.[48] In a typical synthesis, polyacrylic weak-acid cation-exchanged resin (PWAC) was added to aqueous $FeCl_2 \cdot 4H_2O$ or $FeCl_3 \cdot 6H_2O$. Next, the solution was stirred for a certain time under nitrogen protection. Then, the solid was collected by centrifugation and washed with deionized water for two times. Finally, the solid was carbonized at 1000 °C for 1 h under N_2. In order to remove the Fe species, the obtained product was treated with 10% hydrochloric acid for 8 h. The solids were separated by centrifuge and washed several times with deionized water, and then dried in vacuum oven at 80 °C for 6 h. Five CNS supports were obtained controlled by adjusting the reaction time in aqueous $FeCl_2 \cdot 4H_2O$ or $FeCl_3 \cdot 6H_2O$ solution, denoted as CNS-1 ($FeCl_3 \cdot 6H_2O$, 3 h), CNS-2 ($FeCl_2 \cdot 4H_2O$, 1.5 h), CNS-3 ($FeCl_2 \cdot 4H_2O$, 3 h), CNS-4 ($FeCl_2 \cdot 4H_2O$, 6 h), CNS-5 ($FeCl_2 \cdot 4H_2O$, 12 h), respectively.

Preparation of 3.5 wt% Pt/CNS catalysts. The 3.5 wt% Pt/CNS catalysts were obtained through a simple borohydride reduction method. CNS (0.500 g) support was added to 50 mL of deionized water and subjected to ultrasonic treatment for 30 min. Then, $H_2PtCl_6 \cdot 6H_2O$ aqueous solution (4.65 g, Pt content: 3.76 mg g^{-1}) was added into the mixture. The resultant solution was further sonicated for 30 min. Subsequently, the slurry was transferred to an ice bath (2–4 °C) and stirred vigorously for 30 min. In addition, the slurry pH was adjusted to 8.0 using NaOH (0.1 mol L^{-1}) solution. Afterwards, an excess of $NaBH_4$ (0.2 mol L^{-1}) solution was added to the mixture, and stirred for 3 h. The mixture was statically placed in an ice bath for 10 h. Finally, 3.5 wt% Pt/CNS catalysts were obtained after filtrating, washing with deionized water and ethanol until no chloride ions detected and drying at 60 °C for 10 h. The 3.5 wt% Pd/CNS catalysts were prepared by following the same method. $PdCl_2$ aqueous solution (5.00 g, Pd content: 3.50 mg g^{-1}) was added into the mixture of CNS (0.500 g) support and 50 mL of deionized water.

Catalyst characterization

X-ray diffraction (XRD) patterns were obtained with a Rigaku D/max-IIIB diffractometer by using Cu-K_α ($\lambda = 1.5406$ Å) radiation. The accelerating voltage and applied current were 40 kV and 20 mA, respectively. Raman spectra were recorded with a Jobin Yvon HR 800 micro-Raman spectrometer at 457.9 nm. The laser beam was focused on the sample with a 50× objective. Transmission electron microscopy (TEM) was carried out with a JOEL model JEM-2100 electron microscope working at an acceleration voltage of 200 kV. The samples for TEM were suspended in ethanol and supported onto a holey carbon film on a Cu grid. X-ray photoemission spectroscopy (XPS) was carried out on a Kratos-AXIS ULTRA DLD with an Al-K_α radiation source. Scanning electron microscopy (SEM) was measured on a Hitachi S-4800 field emission electron microscope operating at 20 kV. Surface area was measured at 77 K with a Micromeritics Tristar II 3020 analyzer. The sample was degassed under vacuum at 423 K for 4 h prior to measurements. The Brunauer–Emmett–Teller (BET) method was utilized to calculate the specific surface areas using adsorption data in a relative pressure range from 0.05 to 0.25. The content of platinum and palladium in the catalysts was determined by inductively coupled plasma-optical emission spectrometry (ICP-OES), which was performed by a Perkin Elmer Optima 7000 DV analyzer. Before the measurement, each sample was dissolved in a diluted HF and chloroazotic acid solution.

Catalytic performance evaluation

Catalytic performances of catalysts for the hydrogenation of CAL were carried out in a 100 mL autoclave. In brief, 50 mg of catalysts were immersed into 15 mL of isopropanol. The trace of dissolved oxygen was removed by flushing with nitrogen and hydrogen at 5 bar for 3 times, respectively. The temperature was raised to 110 °C under 10 bar of hydrogen for 1 h to re-activate the catalysts. A mixture of CAL (1.0 g) and isopropanol (15 mL) was added into the autoclave. After flushing with nitrogen at 5 bar for 3 times and subsequently with hydrogen at 5 bar for 3 times, the reaction was allowed to proceed at 60 °C under 10 bar of hydrogen for 2 h. The products were analyzed on a gas chromatography (Agilent 7820A) equipped with an FID detector and an HP-5 capillary column (30 m × 0.32 mm × 0.25 μm).

The turnover frequency (TOF) for the catalysts was calculated by using eqn (1) at a CAL conversion.[49]

$$\mathrm{TOF} = \frac{n(\mathrm{CAL}) \times \mathrm{conv.}\%}{[m(cat)y(\mathrm{Pt})/M(\mathrm{Pt})] \times D(\mathrm{Pt}) \times t} \quad (1)$$

where n(CAL), m(cat), y(Pt) and M(Pt) represent the mole of CAL, the catalyst weight, Pt loading level, and molar mass, respectively, while conv.% and t are the conversion of CAL and the reaction time, respectively. D(Pt) is the dispersion of surface Pt sites and is estimated from the mean particle size of Pt.[50,51]

Results and discussion

In order to prepare carbon nanosheets (CNS) support with different graphitization degree, Fe species (Fe^{2+} and Fe^{3+}) was chosen as graphitization catalyst to form the graphene-like structure.[48] XRD patterns of the obtained CNS supports exhibit four peaks at 27.0° (002), 42.5° (100), 54.6° (004) and 77.4° (110) which are characteristic facets of graphite (Fig. S1†). From CNS-1 to CNS-5, the graphitization degree of CNS support increases according to the I_G/I_D values of the Raman spectra for five CNS supports (Fig. S2†). SEM images of five CNS supports show carbon nanosheets morphology with flawed and not flat (Fig. S3†). Combined above characterizations, carbon nanosheets with different graphitization degree were successfully prepared as support. No Fe species was observed by XPS of Pt/CNS and Pd/CNS catalysts (Fig. S4†), suggesting Fe was removed by 10% hydrochloric acid in the preparation process of CNS.

XRD analysis

XRD patterns of the Pt/CNS catalysts exhibit a sharp and strong diffraction peak at 27.0°, which corresponds to the facet (002) of graphite (Fig. 1).[48] It suggests that the CNS supports have an ordered structure and high graphitization degree. More importantly, the peak intensity increased with treatment time in $FeCl_2 \cdot 4H_2O$, indicating that the graphitization degree of CNS supports can be well controlled. Other diffraction peaks observed in the patterns of all catalysts at 2θ of 39.7, 46.4, and 67.5° can be assigned to the crystalline planes (111), (200), and (220) of the face-centered cubic Pt nanoparticles, respectively (Fig. 1).[52] The averaged crystal sizes of Pt nanoparticles calculated by full width at half maximum of Pt (111) reflection based on Scherrer's equation[53] are 5.2, 5.4, 5.0, 5.2 and 5.0 nm for Pt/CNS-1, Pt/CNS-2, Pt/CNS-3, Pt/CNS-4 and Pt/CNS-5 samples, respectively (Table 1). It confirms that the particle size of Pt is same for five samples. The Pt loading was about 3.5 wt% ± 0.2% for the five Pt/CNS samples based on ICP-OES. These catalysts possess similar BET surface area of 56.5–60.1 $m^2\ g^{-1}$. The metal dispersion was estimated based on the mean size of Pt particles (equal to 1.13/mean size) assuming a cuboctahedral shape of the metal particles were 21.7%, 20.9%, 22.6%, 21.7% and 22.6% for Pt/CNS-1, Pt/CNS-2, Pt/CNS-3, Pt/CNS-4 and Pt/CNS-5, respectively (Table 1).[51,54]

Raman spectroscopy

Raman is one of useful tools to provide structure details of carbon materials, such as disorder and defect structure. In the Raman spectra of the as-obtained Pt/CNS catalysts (Fig. 2), two prominent peaks at 1368 and 1590 cm^{-1} were observed, which were well assigned to the breathing mode of κ-point phonons of A_{1g} symmetry (D band) and E_{2g} phonons of sp^2 carbon atoms (G band), respectively.[55] It is well known that a high value in the

Table 1 Physicochemical property of the as-obtained Pt/CNS catalysts

Catalyst	S_{BET}[a] ($m^2\ g^{-1}$)	Pt crystal size[b] (nm)	Pt dispersion[c] (%)	I_G/I_D[d]
Pt/CNS-1	60.1	5.2	21.7	1.9
Pt/CNS-2	59.4	5.4	20.9	3.5
Pt/CNS-3	59.7	5.0	22.6	4.3
Pt/CNS-4	58.6	5.2	21.7	4.9
Pt/CNS-5	56.5	5.0	22.6	6.7

[a] BET surface area. [b] Calculated from Pt(111) in XRD patterns based on Scherrer's equation. [c] Estimated from the mean particle size of Pt. [d] Calculated from the Raman spectra according to the intensities of D and G peaks.

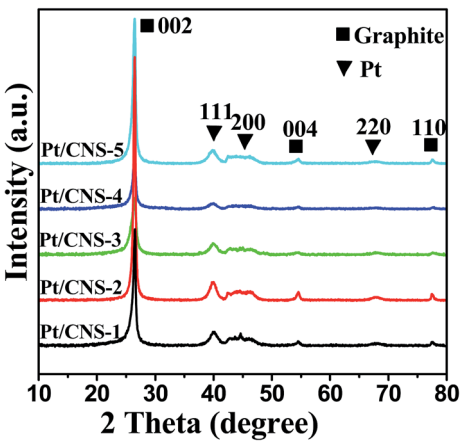

Fig. 1 XRD patterns of Pt/CNS-1, Pt/CNS-2, Pt/CNS-3, Pt/CNS-4 and Pt/CNS-5 catalysts.

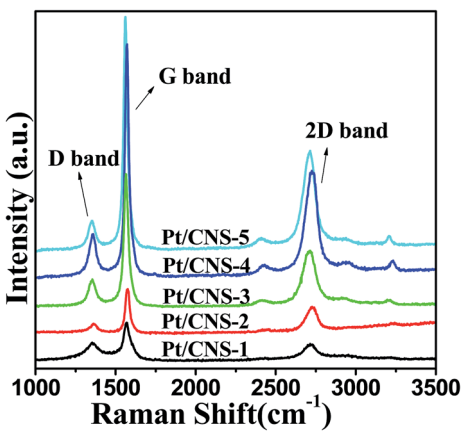

Fig. 2 Raman spectra of Pt/CNS-1, Pt/CNS-2, Pt/CNS-3, Pt/CNS-4 and Pt/CNS-5 catalysts.

intensity ratio of G to D (I_G/I_D) indicates a better degree of graphitization in the carbon materials. The I_G/I_D values for Pt/CNS-1, Pt/CNS-2, Pt/CNS-3, Pt/CNS-4 and Pt/CNS-5 catalysts are calculated to be 1.9, 3.5, 4.3, 4.9, and 6.7, respectively. It suggests that the graphitization degree of CNS support increases from Pt/CNS-1 to Pt/CNS-5, which is in good agreement with the XRD results. Raman and XRD results confirm the obtained Pt/CNS catalysts with different graphitization degree for CNS supports.

TEM analysis

TEM analysis provided more detailed information about the particle dispersion and particle size of the Pt/CNS catalysts. TEM images (Fig. 3a, d and g) of Pt/CNS-1, Pt/CNS-3, and Pt/CNS-5 catalysts clearly show that Pt NPs are well dispersed on CNS support. HRTEM images of Pt/CNS-1, Pt/CNS-3 and Pt/CNS-5 catalysts (Fig. 3b, c, e, f, h and i) disclose that high crystalline Pt NPs closely contact with CNS support. The thin layer edges of carbon nanosheets were observed clearly (Fig. 3b, e and h). The two kind of well-defined lattice fringes can be clearly observed in Fig. 3c, f and i. The measured lattice spacing value of Pt NPs and CNS support is 0.223–0.227 and 0.352–0.379 nm (Fig. 3c, f and i), which can be well assigned to the planes (111) of the face-centered cubic Pt and the (002) planes of graphite, respectively. This explains that the Pt/CNS catalysts have a graphitic structure.

In addition, with the increase in graphitization degree of CNS supports, the layer edges of carbon nanosheets and the lattice spacing were much clearer. From Fig. 3, it can be seen that the Pt/CNS-5 catalyst have a better graphitic structure than Pt/CNS-1 and Pt/CNS-3. These analyses prove that the Pt/CNS materials with graphitic structures were successfully synthesized. The corresponding particle size distributions (Fig. 3j–l) reveal that the average particle sizes of Pt NPs are 4.9, 4.8, and 5.4 nm for Pt/

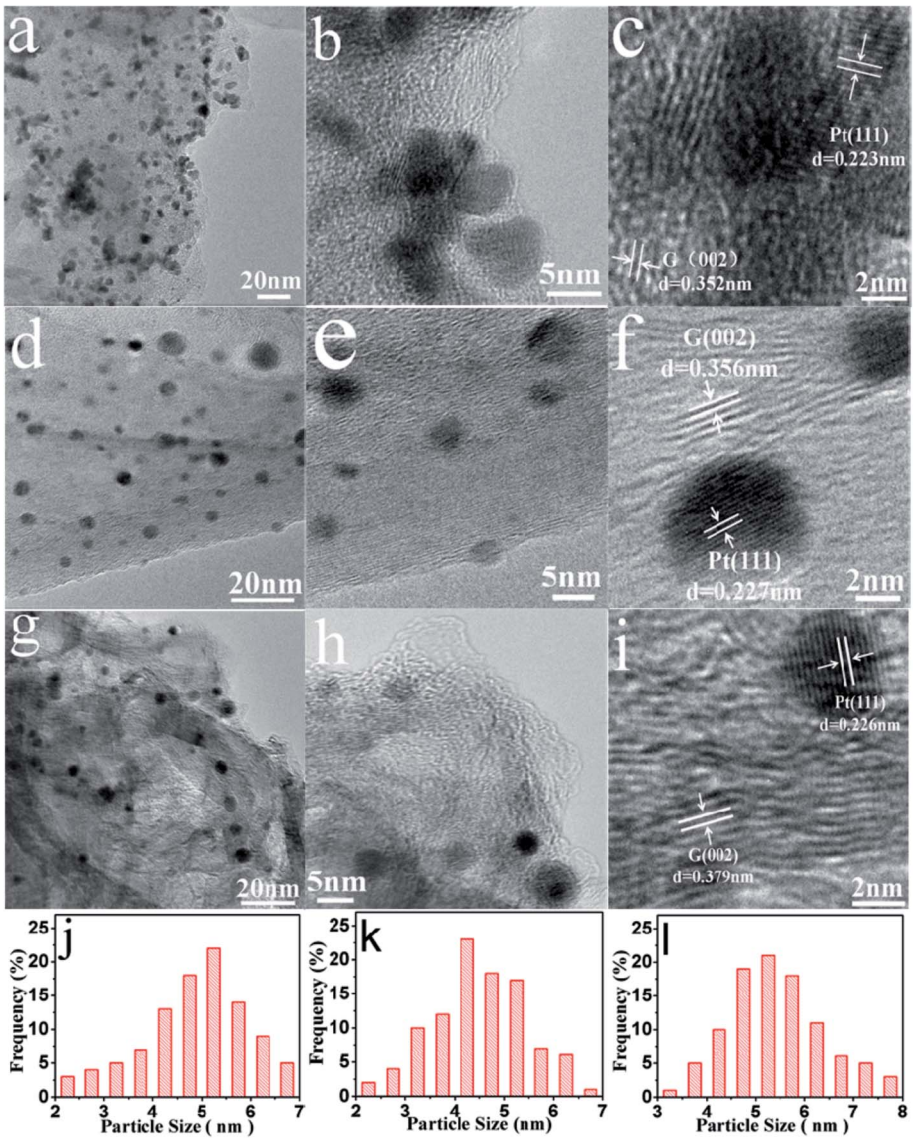

Fig. 3 TEM images, HRTEM images and corresponding particle size distribution plots of (a–c, j) Pt/CNS-1, (d–f, k) Pt/CNS-3 and (g–i, l) Pt/CNS-5 catalysts. The average diameters obtained by measuring about 100 particles for each catalyst.

CNS-1, Pt/CNS-3 and Pt/CNS-5, respectively. The results are well consistent with the calculated results based on Scherrer's equation from XRD patterns.

X-ray photoelectron spectroscopy

The C 1s spectra of XPS have been analyzed and shown in Fig. 4. From the C 1s spectra of five samples, four different peaks centered at about 284.5, 285.7, 287.9 and 289.7 eV were observed, corresponding to C–C, C–O, C═O and O–C═O groups, respectively (Fig. 5).[45,46] Based on the integration of corresponding peaks, the percentage of sp^2 hybridized C–C bonds were 32.4%, 42.4%, 44.1%, 46.2% and 49.7%, respectively. It is in good agreement with the Raman results. It also proves that graphitization degree increase for the supports from CNS-1 to CNS-5.

XPS was used to study the surface Pt species of Pt/CNS catalysts (Fig. 5). It is clearly found that Pt 4f signal consists of three chemically different species from the spin-split obtained by fitting Gaussian peaks after Shirley-background subtraction. The most intense pair of peaks (71.4 and 74.7 eV), the second doublet (72.6 and 75.9 eV) and the third doublet (74.9 and 78.0 eV) can be assigned to metallic Pt^0, Pt^{2+} in the form of PtO and $Pt(OH)_2$, and Pt^{4+} possibly in the form of PtO_2, respectively,[56–59] as summarized in Table 2. The binding energy of metallic Pt^0 is high due to Pt–C strong interaction, resulting in a fast electron transfer from Pt to CNS. In terms of quantitation of the composition of the Pt nanoparticles, the content of the surface Pt^0 species was estimated to be 50.8%, 54.0%, 54.8%, 57.8% and 67.2% for Pt/CNS-1, Pt/CNS-2, Pt/CNS-3, Pt/CNS-4 and Pt/CNS-5, respectively (Table 2), which demonstrates the amount of the Pt^0 species increases from Pt/CNS-1 to Pt/CNS-5. However, the changed degree in the surface Pt^0 content is slight Pt/CNS-1 to Pt/CNS-4, suggesting they have similar Pt^0 content.

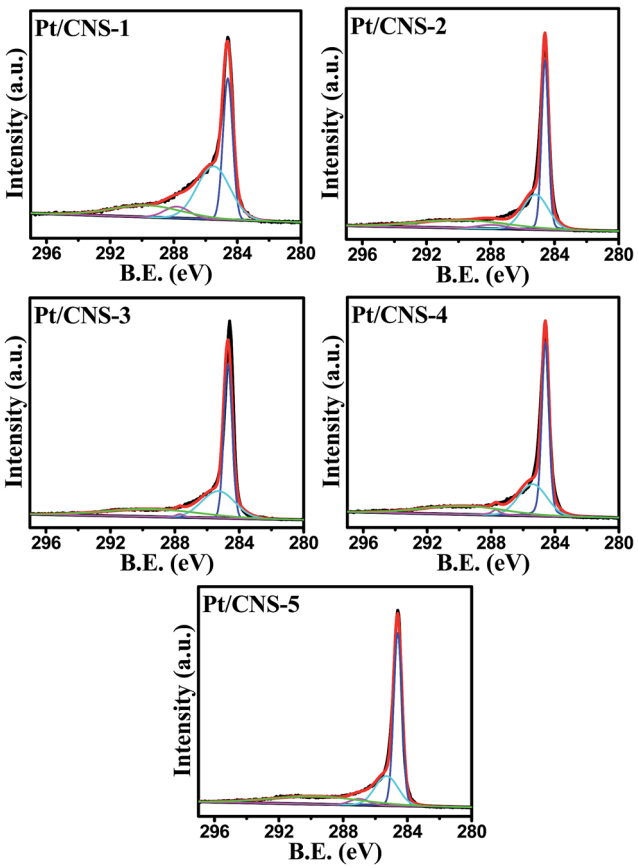

Fig. 4 C 1s high-resolution XPS spectra of Pt/CNS-1, Pt/CNS-2, Pt/CNS-3, Pt/CNS-4, and Pt/CNS-5 catalysts.

Catalytic performances

The Pt/CNS catalysts were applied for the selective hydrogenation of CAL. The major products obtained by the hydrogenation

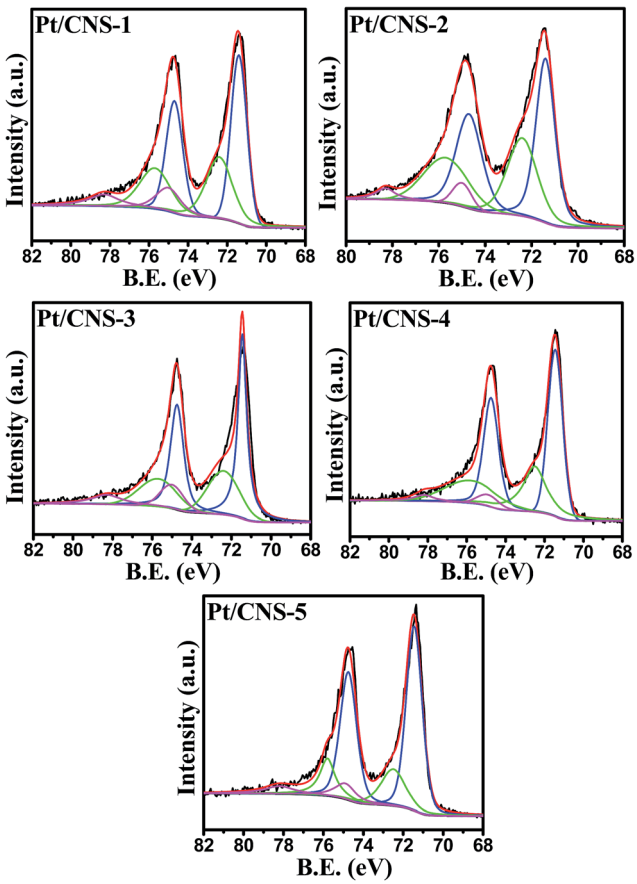

Fig. 5 Pt 4f high-resolution XPS spectra of Pt/CNS-1, Pt/CNS-2, Pt/CNS-3, Pt/CNS-4, and Pt/CNS-5 catalysts.

Table 2 XPS data of distributions of functional groups

	C species content[a] (%)				Pt species content[a] (%)		
Catalyst	C═C	C–O	C═O	O–C═O	Pt^0	Pt^{2+}	Pt^{4+}
Pt/CNS-1	32.4	41.4	6.8	19.4	50.8	35.8	13.4
Pt/CNS-2	42.4	30.2	3.6	23.8	54.0	39.4	6.6
Pt/CNS-3	44.1	30.5	1.1	24.3	54.8	32.1	13.1
Pt/CNS-4	46.2	29.5	2.1	22.2	57.8	36.5	5.7
Pt/CNS-5	49.7	22.9	3.9	23.5	67.2	23.2	9.6

[a] Calculated from the XPS results.

of CAL involve COL, HALD and HALC (Table 3). In order to clear disclose the effect of CNS supports with different graphitization degree for Pt/CNS catalysts on the conversion and selectivity in the hydrogenation reaction of CAL, the evaluated experiments of catalytic performance were carried out under mild reaction conditions (10 bar H_2 at 60 °C for 2 h). The conversion of CAL is 14.4%, 16.1%, 24.3%, 43.5% and 58.7% over Pt/CNS-1, Pt/CNS-2, Pt/CNS-3, Pt/CNS-4, and Pt/CNS-5, respectively. The turnover frequency (TOF) were 7.76, 9.01, 12.6, 23.4 and 30.4 s^{-1} for Pt/CNS-1, Pt/CNS-2, Pt/CNS-3, Pt/CNS-4, and Pt/CNS-5, respectively. Meanwhile, the selectivity to COL also increases from Pt/CNS-1 (16.7%) to Pt/CNS-5 (67.3%), in which the highest selectivity towards COL was obtained over the Pt/CNS-5 catalyst. When the reaction was performed at 80 °C under 10 bar H_2 for 4 h, CAL conversion and selectivity to COL can reach 87.5% and 90.5% over Pt/CNS-5, respectively.

A serial of experiments about the traces of conversion and selectivity as a function of reaction time were also carried out over the Pt/CNS catalysts and the results are display in Fig. 6 and 7. At initial 20 min, the conversion of CAL was less than 8% for all Pt/CNS catalyst. After a reaction time of 60 min, the conversion of CAL increased to 8.9%, 9.1%, 10.3%, 14.6% and 33.1% over Pt/CNS-1, Pt/CNS-2, Pt/CNS-3, Pt/CNS-4 and Pt/CNS-5, respectively. And the selectivity to COL was 17.0%, 24.6%, 42.3%, 60.7% and 69.4% over Pt/CNS-1, Pt/CNS-2, Pt/CNS-3, Pt/CNS-4, and Pt/CNS-5, respectively. On the whole, the conversion of CAL increases gradually with time, and the selectivity to COL slightly decreases in 120 min.

The recycling experiments were performed over Pt/CNS-5 based on its better catalytic activity. The catalyst was reused directly without any treatment after precipitated and separated from the reaction solution. In every run, the activity exhibited a slight decrease compared with the results last run. After four used cycles, the conversion of CAL declined from 58.7% to 45%, and the selectivity to COL decreased from 67.3% to 46.5% (Fig. 8). According our previous studies,[16,43] the deactivation reasons can be attributed to the aggregation of Pt particles, the reduced amount of Pt^0 species on the surface and the formed side product with large molecular weights adsorbed on the active sites.

Table 3 Catalytic performances of Pt/CNS catalysts

Catalysts	Conversion (%)	TOF[c] (s^{-1})	Selectivity (%)			
			HALD	HALC	COL	Others[d]
Pt/CNS-1[a]	14.4	7.76	1.0	2.7	16.7	79.6
Pt/CNS-2[a]	16.1	9.01	1.2	2.5	21.9	74.4
Pt/CNS-3[a]	24.3	12.6	1.5	1.6	41.6	55.3
Pt/CNS-4[a]	43.5	23.4	3.9	2.0	58.9	35.2
Pt/CNS-5[a]	58.7	30.4	2.9	2.2	67.3	27.6
Pt/CNS-5[b]	87.5	22.7	1.3	1.8	90.5	6.4

[a] Reaction conditions: under 10 bar H_2 at 60 °C for 2 h. [b] Reaction conditions: under 10 bar H_2 at 80 °C for 4 h. [c] Calculated at CAL conversion. [d] Includes 1-(3-propoxyprop-1-enyl)benzene, cinnamyl formate, cinnamic acid, benzyl, cinnamate, 4,4-diphenylcyclohexa-1,5-dienyl acetate, and other condensation products that could not be identified by GC-MS because of their large molecular weights.

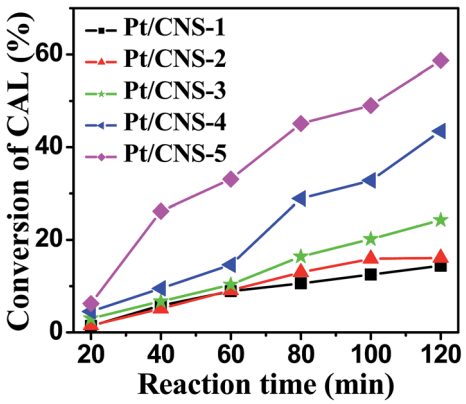

Fig. 6 Cinnamaldehyde conversion *versus* reaction time in cinnamaldehyde hydrogenation over Pt/CNS-1, Pt/CNS-2, Pt/CNS-3, Pt/CNS-4, and Pt/CNS-5 catalysts (reaction conditions: 50 mg 3.5 wt% Pt/CNTs, 1.00 g CAL, 30 mL isopropanol, 10 bar H_2, 60 °C, 2 h).

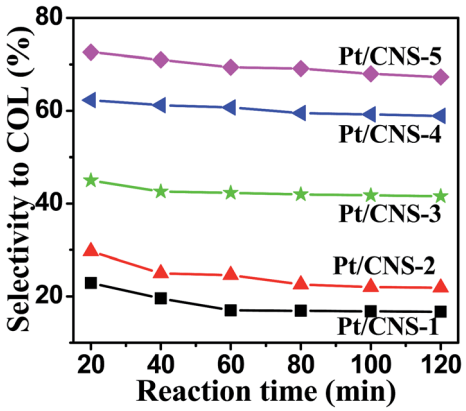

Fig. 7 Selectivity as a function of reaction time of Pt/CNS-1, Pt/CNS-2, Pt/CNS-3, Pt/CNS-4, and Pt/CNS-5 catalysts (reaction conditions: 50 mg 3.5 wt% Pt/CNTs, 1.00 g CAL, 30 mL isopropanol, 10 bar H_2, 60 °C, 2 h).

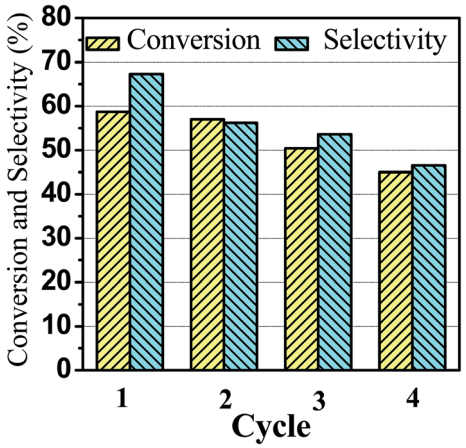

Fig. 8 Stability test of Pt/CNS-5 (reaction conditions: 50 mg 3.5 wt% Pt/CNTs, 1.00 g CAL, 30 mL isopropanol, 10 bar H_2, 60 °C, 2 h).

It is noticed that the order of conversion to CAL and selectivity to COL is Pt/CNS-5 > Pt/CNS-4 > Pt/CNS-3 > Pt/CNS-2 > Pt/CNS-1. According to above characterization results, Pt/CNS catalysts with similar Pt content and mean particle size values of Pt were obtained by supporting Pt on CNS with different graphitization degree. Thus, the effect of Pt content and its mean particle size on the catalytic activity should be excluded for these Pt/CNS catalysts in this study. In our previous studies,[16,43,60] the amount of surface Pt^0 species was considered as a key species in responsibility of the selectivity to COL. In addition, Wang *et al.* found Pt^{2+} species played an important role on the selectivity to COL when the ratio of Pt^{2+} to Pt (Pt^{2+}/Pt) is more than 1.0.[56] However, in our studies, the content of Pt^0 species is more than that of Pt^{2+} species, which the effect of Pt^{2+} species on the activity and selectivity can be ignored. Generally, Pt^{4+} species can lead to form the undesired condensation products due to its acidity. Thus, Pt^0 species should play the dominant role in selective hydrogenation of CAL. The more surface Pt^0 content catalyst has, the higher selectivity to COL it exhibits. In general, the Pt^0 content increases with graphitization degree of CNS support from Pt/CNS-1 to Pt/CNS-5 according to the results of XPS (Fig. 5), XRD (Fig. 1) and Raman (Fig. 2). The change of the amount of the Pt^0 species among these Pt/CNS catalysts can be ascribed to the difference in the interaction between Pt and CNS support with different graphitization degree. A large amount of C–OH, COOH and C=O groups existing on the CNS with much lower graphitization degree result to the transfer of more electrons from Pt to CNS support,[61] which would lead to the formation of high oxidation state Pt species (Pt^{2+} and Pt^{4+}) and the decrease in the content of Pt^0 species. The work by Guo *et al.* also confirmed it.[62] They studied the effect of the surface properties of the carbon nanotube (CNT) support on the hydrogenation results of CAL. Their results showed the conversion and selectivity for hydrogenation of CAL highly depended on the surface properties of the CNT support over Pt/CNT catalyst. Removal of oxygen-containing groups from CNT surfaces elevated both activity and selectivity, due to the suppressed side reactions catalyzed by acid and enhanced electron transfer from CNT to Pt nanoparticles.[62] In other word, with the increase in graphitization degree of support, fewer and fewer oxygen-containing groups on the support surface can enhance the transfer of electron from CNS support to Pt. The enriched electron density surrounding the Pt nanoparticles reduces the probability of C=C bond coordinated to Pt active sites due to the electronic repulsion, thereby increases the selectivity toward COL.[18]

The highest selectivity and conversion can be attributed to the largest amount of Pt^0 species on the surface the Pt/CNS-5 sample.[12,58] It can be seen that the selectivity to COL increased from 16.7% to 58.9% with graphitization degree of CNS support for Pt/CNS-1, Pt/CNS-2, Pt/CNS-3 and Pt/CNS-4. However, the Pt^0 content increases slightly about 7% from Pt/CNS-1 to Pt/CNS-4. Therefore, we think that the difference in conversion to CAL and selectivity to COL for the Pt/CNS catalysts should be also relate to the adsorbed property of different CNS supports for CAL. The better graphitized degree carbon nanosheets support is, the higher adsorption *capacity* for CAL it shows on its surface. The well graphitization degree of CNS support is advantage of the strong π–π interactions between CAL and the surface sp^2-bonded of CNS support, which results to the high conversion of CAL.[63] Moreover, the high π–π interactions can favor of the contact of C=O with Pt species due to CAL structure, which leads to the increase in selectivity to COL.[41]

The best catalytic activity and selectivity over Pt/CNS-5 can be attributed to the highest graphitization degree of CNS-5 support. So it can see clearly that the graphitization degree of carbon nanosheets support plays an important role on the selective hydrogenation of CAL.[14] Therefore, the different catalytic activity and selectivity over the Pt/CNS catalysts are attributed to the surface Pt^0 content and the adsorption *capacity* for CAL on the catalyst surface that are closely related to the graphitization degree of CNS.

Generally, Pd is favor of hydrogenation of C=C in the selective hydrogenation of CAL.[25] In order to confirm above standpoint, we prepared a series of Pd NPs supported on different graphitized carbon nanosheets supports (Pd/CNS) to study the effect of different graphitized CNS supports on the selective hydrogenation of CAL. The results of selective hydrogenation of CAL are displayed in Table 4 over Pd/CNS. The conversion of CAL for Pd/CNS-1, Pd/CNS-2, Pd/CNS-3, Pd/CNS-4 and Pd/CNS-5 was 24.4%, 37.4%, 42.4%, 56.8% and 59.1%, respectively, when the reaction was carried out under 10 bar H_2 at 60 °C for 2 h (Table 4). Meanwhile, HALD was main product and its selectivity also increased as the rise of graphitization degree of CNS supports. The Pd/CNS-5 catalyst showed the highest selectivity (~65.3%) towards HALD among the five catalysts. The turnover frequency (TOF) was 13.4, 21.6, 24.2, 32.1 and 32.8 s^{-1} for Pd/CNS-1, Pd/CNS-2, Pd/CNS-3, Pd/CNS-4 and Pd/CNS-5, respectively.

The similar mean particle size (~10 nm) of Pd was obtained for all Pd/CNS catalysts from XRD results (Fig. S5†). Hence, the effect of mean particle size of Pd on catalytic activity should be also excluded for these Pd/CNS catalysts. It has been found that the Pd^0 species plays a key role on the selectivity to HALD in the selective hydrogenation of cinnamaldhyde.[25] The amount of Pd^0 species is 32.5%, 40.7%, 49.4%, 59.6% and 62.4% on the surface of Pd/CNS-1, Pd/CNS-2, Pd/CNS-3, Pd/CNS-4 and Pd/CNS-5, respectively (Table S1 and Fig. S6†), which

Table 4 The catalytic performances of Pd/CNS catalysts

			Selectivity (%)			
Catalysts	Conversion (%)	TOF[a] (s^{-1})	HALD	HALC	COL	Others[b]
Pd/CNS-1	24.4	13.4	36.4	14.3	3.1	46.2
Pd/CNS-2	37.4	21.6	48.7	15.7	3.9	31.7
Pd/CNS-3	42.4	24.2	53.4	17.9	2.7	26.0
Pd/CNS-4	56.8	32.1	58.7	21.0	0	20.3
Pd/CNS-5	59.1	32.8	65.3	9.8	3.9	21.0

[a] Calculated at CAL conversion. [b] Includes 1-(3-propoxyprop-1-enyl) benzene, cinnamyl formate, cinnamic acid, benzyl, cinnamate, 4,4-diphenylcyclohexa-1,5-dienyl acetate, and other condensation products that could not be identified by GC-MS because of their large molecular weights.

demonstrate that high graphitized degree of CNS is advantage of formation of the surface Pd^0 species due to enhancing the electron transfer from CNS support to Pd. The Pd/CNS-5 catalyst shows the highest conversion (~59.1%) and the highest selectivity (~65.3%) towards HALD. And the other main reason is that the different graphitized carbon nanosheets supports play other roles on the conversion of CAL. The better graphitized carbon nanosheets support is, the more adsorption of CAL is on its surface. Although the strong π–π interactions is also advantage of the contact of C=O with Pd species, the hydrogenation activity of Pd for C=O is much weaker than for C=C. Thus, the main product was still HALD by the hydrogenation C=C of CAL over Pd/CNS catalyst. Therefore, the high catalytic activity can be attributed to the high graphitization degree of CNS support. The results confirm further the effect of graphitization degree on noble metal species and activity for selective hydrogenation of CAL.

Conclusions

In summary, different graphitized carbon nanosheets materials were investigated as a support for Pt and Pd catalysts for the selective hydrogenation of CAL. The graphitization degree of CNS supports can be well controlled by the amount of growth catalysts (Fe species). The Pt/CNS and Pd/CNS catalysts have nanosheets structures, highly dispersed Pt nanoparticles with a particle size of ~5 nm and Pd nanoparticles with a particle size of ~10 nm, respectively. The activity and selectivity of Pt/CNS and Pd/CNS catalysts increases as the rise of graphitization degree. The different catalytic activity and selectivity over the Pt/CNS and Pd/CNS catalysts are attributed to the surface Pt^0 and Pd^0 content and the adsorption *capacity* for CAL on the catalyst surface that are closely related to the graphitization degree of CNS.

Acknowledgements

This work was supported by Natural Sciences Fund of Heilongjiang Province (B2015009), the Innovative Research Project of Key Laboratory of Functional Inorganic Material Chemistry (Heilongjiang University), Ministry of Education (2015), the Scientific Research Foundation for the Returned Overseas Chinese Scholars, State Education Ministry (2013-1792) and Ministry of Human Resources and Social Security (2013-277).

References

1 F. Zaera, *J. Phys. Chem. B*, 2002, **106**, 4043–4052.
2 R. J. White, R. Luque, V. L. Budarin, J. H. Clark and D. J. Macquarrie, *Chem. Soc. Rev.*, 2009, **38**, 481–494.
3 G. A. Somorjai and J. Y. Park, *Angew. Chem., Int. Ed.*, 2008, **47**, 9212–9228.
4 G. Wienhöfer, F. A. Westerhaus, K. Junge, R. Ludwig and M. Beller, *Chem.–Eur. J.*, 2013, **19**, 7701–7707.
5 B. Wu, H. Huang, J. Yang, N. Zheng and G. Fu, *Angew. Chem., Int. Ed.*, 2012, **51**, 3440–3443.
6 S. Fleischer, S. Zhou, K. Junge and M. Beller, *Angew. Chem., Int. Ed.*, 2013, **52**, 5120–5124.
7 Z. Y. Guo, C. X. Xiao, R. V. Maligal-Ganesh, L. Zhou, T. W. Goh, X. Li, D. Tesfagaber, A. Thiel and W. Huang, *ACS Catal.*, 2014, **4**, 1340–1348.
8 G. R. Bertolini, C. I. Cabello, M. Muñoz, M. Casella, D. Gazzoli, I. Pettiti and G. Ferraris, *J. Mol. Catal. A: Chem.*, 2013, **366**, 109–115.
9 M. G. Prakash, R. Mahalakshmy, K. R. Krishnamurthy and B. Viswanathan, *Catal. Today*, 2016, **263**, 105–111.
10 Z. B. Tian, Q. Y. Li, J. Y. Hou, L. Pei, Y. Li and S. Y. Ai, *J. Catal.*, 2015, **331**, 193–202.
11 L. J. Durndell, C. M. A. Parlett, N. S. Hondow, M. A. Isaacs, K. Wilson and A. F. Lee, *Sci. Rep.*, 2015, **5**, 9425.
12 P. Gallezot and D. Richard, *Catal. Rev.: Sci. Eng.*, 1998, **40**, 81–126.
13 P. Claus, *Top. Catal.*, 1998, **5**, 51–62.
14 P. Mäki-Arvela, J. Hájek, T. Salmi and D. Y. Murzin, *Appl. Catal., A*, 2005, **292**, 1–49.
15 Z. Broučková, M. Czaková and M. Čapka, *J. Mol. Catal.*, 1985, **30**, 241–249.
16 D. Wang, Y. J. Zhu, C. G. Tian, L. Wang, W. Zhou, Y. L. Dong, Q. Han, Y. F. Liu, F. L. Yuan and H. G. Fu, *Catal. Sci. Technol.*, 2015, **109**, 2403–2412.
17 T. Mitsudome and K. Kaneda, *Green Chem.*, 2013, **15**, 2636–2654.
18 H. Vu, F. Gonçalves, R. Philippe, E. Lamouroux, M. Corrias, Y. Kihn, D. Plee, P. Kalck and P. Serp, *J. Catal.*, 2006, **240**, 18–22.
19 C. Rudolf, B. Dragoi, A. Ungureanu, A. Chirieac, S. Royer, A. Nastro and E. Dumitriu, *Catal. Sci. Technol.*, 2014, **4**, 179–189.
20 T. Szumelda, A. Drelinkiewicz, R. Kosydar and J. Gurgul, *Appl. Catal., A*, 2014, **487**, 1–15.
21 W. W. Lin, H. Y. Cheng, L. M. He, Y. C. Yu and F. Y. Zhao, *J. Catal.*, 2013, **303**, 110–116.
22 H. Wang, Y. Y. Shu, M. Y. Zheng and T. Zhang, *Catal. Lett.*, 2008, **124**, 219–225.
23 Y. J. Zhu and F. Zaera, *Catal. Sci. Technol.*, 2014, **4**, 955–962.
24 M. G. Prakash, R. Mahalakshmy, K. R. Krishnamurthy and B. Viswanathan, *Catal. Sci. Technol.*, 2015, **5**, 3313–3321.
25 D. Wang, Y. J. Zhu, C. G. Tian, L. Wang, W. Zhou, Y. L. Dong, H. J. Yan and H. G. Fu, *ChemCatChem*, 2016, **8**, 1718–1726.
26 X. Xiang, W. H. He, L. S. Xie and F. Li, *Catal. Sci. Technol.*, 2013, **3**, 2819–2827.
27 J. Teddy, A. Falqui, A. Corrias, D. Carta, P. Lecante, I. Gerber and P. Serp, *J. Catal.*, 2011, **278**, 59–70.
28 N. Mahata, F. R. Goncalves, M. F. Pereira and J. L. Figueiredo, *Appl. Catal., A*, 2008, **339**, 159–168.
29 N. Job, R. Pirard, J. Marien and J. P. Pirard, *Carbon*, 2004, **42**, 619–628.
30 M. S. Ide, B. Hao, M. Neurock and R. J. Davis, *ACS Catal.*, 2012, **2**, 671–683.
31 J. H. Vleeming, B. F. M. Kuster and G. B. Marin, *Catal. Lett.*, 1997, **46**, 187–194.
32 K. Liberková and R. Touroude, *J. Mol. Catal. A: Chem.*, 2002, **180**, 221–230.

33 J. P. Stassi, P. D. Zgolicz, S. R. de Miguel and O. A. Scelza, *J. Catal.*, 2013, **306**, 11–29.
34 X. Yuan, J. W. Zheng, Q. Zhang, S. R. Li, Y. H. Yang and J. L. Gong, *AIChE J.*, 2014, **60**, 3300–3311.
35 Y. Zhao, M. M. Liu, B. B. Fan, Y. F. Chen, W. M. Lv, N. Y. Lu and R. F. Li, *Catal. Commun.*, 2014, **57**, 119–123.
36 S. Bhogeswararao and D. Srinivas, *J. Catal.*, 2012, **285**, 31–40.
37 Z. M. Tian, X. Xiang, L. S. Xie and F. Li, *Ind. Eng. Chem. Res.*, 2013, **52**, 288–296.
38 H. G. Manyar, B. Yang, H. Daly, H. Moor, S. McMonagle, Y. Tao, G. D. Yadav, A. Goguet, P. Hu and C. Hardacre, *ChemCatChem*, 2013, **5**, 506–512.
39 A. Huidobro, A. Sepúlveda-Escribano and F. Rodríguez-Reinoso, *J. Catal.*, 2002, **212**, 94–103.
40 X. Yang, L. P. Wu, L. L. Ma, X. J. Li, T. J. Wang and S. J. Liao, *Catal. Commun.*, 2015, **59**, 184–188.
41 E. V. Ramos-Fernández, A. F. P. Ferreira, A. Sepúlveda-Escribano, F. Kapteijn and F. Rodríguez-Reinoso, *J. Catal.*, 2008, **258**, 52–60.
42 J. J. Shi, R. F. Nie, P. Chen and Z. Y. Hou, *Catal. Commun.*, 2013, **41**, 101–105.
43 X. W. Ji, X. Y. Niu, B. Li, Q. Han, F. L. Yuan, F. Zaera, Y. J. Zhu and H. G. Fu, *ChemCatChem*, 2014, **6**, 3246–3253.
44 L. J. Malobela, J. Heveling, W. G. Augustyn and L. M. Cele, *Ind. Eng. Chem. Res.*, 2014, **53**, 13910–13919.
45 Z. H. Sun, Z. M. Rong, Y. Wang, Y. Xia, W. Q. Du and Y. Wang, *RSC Adv.*, 2014, **4**, 1874–1878.
46 Z. M. Rong, Z. H. Sun, Y. Wang, J. K. Lv and Y. Wang, *Catal. Lett.*, 2014, **144**, 980–986.
47 Q. R. Wang, Y. Y. Wang, Y. F. Zhao, B. Zhang, Y. Y. Niu, X. Xiang and R. F. Chen, *CrystEngComm*, 2015, **17**, 3110–3116.
48 L. Wang, C. Tian, H. Wang, Y. Ma, B. Wang and H. Fu, *J. Phys. Chem. C*, 2010, **114**, 8727–8733.
49 B. F. Machado, S. Morales-Torres, A. F. Pérez-Cadenas, F. J. Maldonado-Hódar, F. Carrasco-Marín, A. M. T. Silva, J. L. Figueiredo and J. L. Faria, *Appl. Catal., A*, 2012, **425–426**, 161–169.
50 X. H. Li, W. L. Zheng, H. Y. Pan, Y. Yu, L. Chen and P. Wu, *J. Catal.*, 2013, **300**, 9–19.
51 A. J. Plomp, H. L. Vuori, A. O. I. Krause, K. P. de Jong and J. H. Bitter, *Appl. Catal., A*, 2008, **351**, 9–15.
52 J. Yang, C. G. Tian, L. Wang and H. G. Fu, *J. Mater. Chem.*, 2011, **21**, 3384–3390.
53 Z. T. Liu, C. X. Wang, Z. W. Liu and J. Lu, *Appl. Catal., A*, 2008, **344**, 114–123.
54 X. H. Li, W. L. Zheng, H. Y. Pan, Y. Yu, L. Chen and P. Wu, *J. Catal.*, 2013, **300**, 9–19.
55 F. Tuinstra and J. L. Koenig, *J. Chem. Phys.*, 1970, **53**, 1126–1130.
56 X. M. Feng, R. M. Li, C. H. Hu and W. H. Hou, *J. Electroanal. Chem.*, 2011, **657**, 28–33.
57 S. Sharma, A. Ganguly, P. Papakonstantinou, X. P. Miao, M. X. Li, J. L. Hutchison, M. Delichatsios and S. Ukleja, *J. Phys. Chem. C*, 2010, **114**, 19459–19466.
58 X. W. Yu and S. Y. Ye, *J. Power Sources*, 2007, **172**, 145–154.
59 Y. Y. Wang, W. H. He, L. R. Wang, J. J. Yang, X. Xiang, B. Zhang and F. Li, *Chem.–Asian J.*, 2015, **10**, 1561–1570.
60 Q. Zheng, D. Wang, F. L. Yuan, Q. Han, Y. L. Dong, Y. F. Liu, X. Y. Niu and Y. J. Zhu, *Catal. Lett.*, 2016, **146**, 1718–1726.
61 S. Handjani, E. Marceau, J. Blanchard, J. M. Krafft, M. Che, P. Mäki-Arvelad, N. Kumard, J. Wärnåd and D. Y. Murzind, *J. Catal.*, 2011, **282**, 228–236.
62 Z. Guo, Y. T. Chen, L. S. Li, X. M. Wang, G. L. Haller and Y. H. Yang, *J. Catal.*, 2010, **276**, 314–326.
63 J. H. Yang, G. Sun, Y. J. Gao, H. B. Zhao, P. Tang, J. Tan, A. H. Lu and D. Ma, *Energy Environ. Sci.*, 2013, **6**, 793–798.